Progress In Electromagnetics Research M, Vol. 56, 71–79, 2017

Dual-Band Composite Wideband Absorbing Material for Broadband Antenna In-Band Radar Cross Section Reduction

Mao Long, Wen Jiang*, and Shu-Xi Gong

Abstract—A composite wideband absorbing material (WAM) covering dual bands is designed, to reduce the in-band radar cross section (RCS) for broadband antenna in this paper. The upper layer is a traditional absorber while the lower one is a dual-band frequency selective surface (FSS), which is formed by a square ring and an improved Jerusalem cross structure. The absorbing band has been broadened to 112% compared with the magnetic sheet without FSS. Over C and X bands, the absorption rate is over 90%. By using the FSS-based WAM as the ground plane of a Vivaldi antenna, substantial RCS reduction is obtained from 2–18 GHz. Moreover, the RCS is reduced remarkably over −80°–80° incident angles except for minority angles, with the radiation performance preserved at the same time. The experimental results are in good agreement with the simulated ones.

1. INTRODUCTION

With the detection and stealth technology developing rapidly, extensive research interest in RCS has been triggered recently. For the purpose of avoiding the detection by enemy's radar, it is of significance to reduce the RCS of sensitive targets such as naval ships and airborne vehicles. For a low observable platform, antenna's scattering signature is of significant contribution to the overall RCS on account of its characteristic to effectively radiate and receive electromagnetic energy. So reducing RCS of the antenna is an effective measure to improve the stealth property of the whole system. While wideband antenna has been critical components in future wireless communications and military applications, controlling and reducing the RCS of wideband antenna are necessary. Thus, materials of low RCS in broadband and wide angles with low-profile configuration are in urgent need. During the past decades, several absorptive methods such as Salisbury screen, resistance loaded electromagnetic band gap (EBG) and absorbing materials (AMs) have been proposed [1–4]. Among them, AM is a practical approach utilized to decrease the RCS signature by means of converting the radio frequency energy into heat. Resistive and resistance-loaded absorbers can broaden the absorption band and enhance the absorptivity through multiple resonances. However, it also brings a lot of instability and inconvenience when combined with antennas [5]. Metamaterial structures presented in [6, 7] obtain good absorbing performance in X-band using tailored unit cells in appropriate dimensions. Nevertheless, the bandwidth and absorption characteristics are insufficient to meet today's military requirement.

Recently, many works on applications of conventional AM and FSS have been carried out [8, 9]. To the readers' knowledge, the bandwidth is not wide enough when FSS or AM is used separately. Studies show that the combination of AM and FSS can expand the absorbing bandwidth of the materials [10, 11]. In [11], two resistive Minkowski fractal loops are employed in order to dissipate energy in a reduced thickness, offering a wide bandwidth from 2.2 GHz to 9.4 GHz, but the loops with continuous sheet resistance are costly. In [12], a WAM is devised to reduce the RCS of a Quasi-Yagi antenna, the

Received 15 February 2017, Accepted 9 April 2017, Scheduled 21 April 2017

* Corresponding author: Wen Jiang (jw13@vip.qq.com).

The authors are with the Collaborative Innovation Center of Information Sensing and Understanding at Xidian University, National Key Laboratory of Antennas and Microwave Technology, Xidian University, Xi'an, Shaanxi 710071, China.

bandwidth is broadened to 94.3%. The absorbing bandwidth is more than 90% in reference [13]. However, the AM's absorbing bandwidth still cannot cover the C and X bands, which have been extensively used in airborne communication.

As a typical printed UWB end-fire antenna, Vivaldi antenna has been widely used for satellite communication, remote sensing, microwave imaging, wideband scanning arrays and high-performance airborne antenna arrays, due to its small dimension, light weight, low fabrication cost, and good radiation characteristic [14, 15]. In order to improve the forward gain, a sheet of metal is usually required to be placed in the vertical position backward of the antenna, which contributes a lot to the RCS. It is precisely the reason that the antenna RCS is on the rise in C and X bands.

For these reasons, a dual-band composite WAM based on FSS is proposed in this paper, the bandwidth of which is broadened to 112%. As a test case, the composite WAM is used as the replacement of the metallic ground of a Vivaldi antenna to obtain in-band RCS reduction. Furthermore, a considerable RCS reduction can be realized in a broadband and over wide incident angles, with the radiation performance preserved at the same time, verifying the reliability and superior performance of the proposed WAM. All simulation work is accomplished by using High Frequency Solution Solver (HFSS) software. The design principle and performance of the composite WAM are analysed in Section 2. In Sections 3 and 4, radiation and scattering performance are given, respectively.

2. DESIGN AND ANALYSED OF COMPOSITE WAM

The unit structure of the composite WAM and the unit form of the loaded FSS are shown in Figure 1(a). The resonant frequency of FSS can be adjusted to be close to that of the AM to form a broader absorbing band. The FSS formed by concentric square ring and an improved Jerusalem cross structure is milled on the top layer of substrate FR4, with a relative permittivity of $\varepsilon_r = 4.4$ and the loss tangent is 0.025, the metal ground is on the bottom layer. The four balls connected with the four strips are used to increase the induction. On top of the FSS is the original gummed rubber AM (TP-15D), whose dielectric constant is $\varepsilon'_r = 20.3$, $\mu'_r = 3.55$, $\tan\delta_D = 0.2266$ and $\tan\delta_M = 0.4422$, extracted by simulation software HFSS.15. The optimized dimensions are given in Table 1.

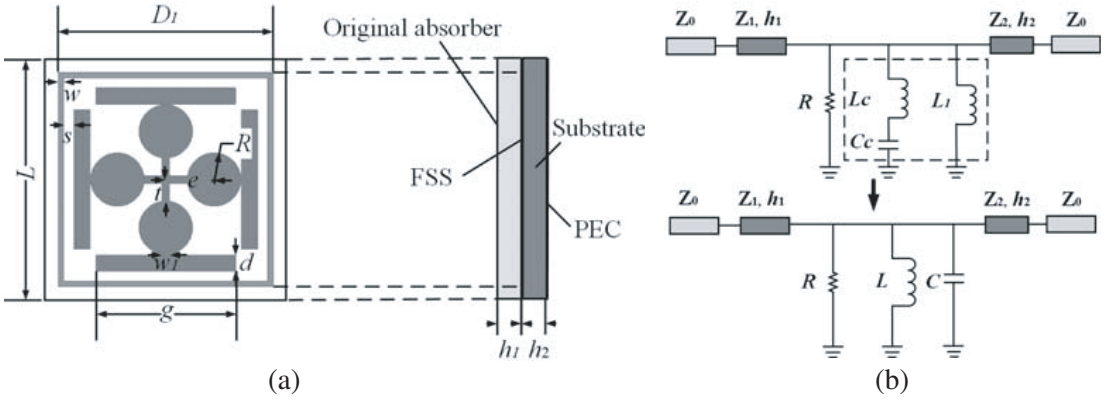

Figure 1. (a) Unit structure of the WAM. (b) Equivalent circuit of the absorbing material.

In [16], an equivalent circuit model of a metamaterial absorber comprising a square-ring-shaped FSS is presented. For the structure of this paper, the length D_1 of the ring and wire width w determine the inductance L_1. The inductance L_C depends on the length $(g + t + \pi R)$ and the width d, while the capacitanceC_C depends on the resonator arm g and the gap s, shown in Figure 1(b) The impedance R is resulted from heat loss and radiation losses of the metal sheet The inductance and capacitance is mainly determined by the structure and size of FSS. The main challenge is to increase resonance peaks in low frequency band without materially increasing the thickness of the absorbing material. The object of this paper is to realize strong absorption over broadband even multiple bands. Based on the equivalent circuit, parameters of the unit cell can be calculated. Parameters of the structure are optimized in Table 1.

Table 1. Parameters of the unit structure (mm).

Parameter	Value	Parameter	Value	Parameter	Value
L	4.5	D_1	3.9	g	2.8
w_1	0.14	h_1	1.2	h_2	1.3
w	0.1	d	0.4	t	0.4
R	0.5	s	0.6	e	0.9

Figure 2(a) shows the reflection coefficient comparison of the original AM, FSS and the composite WAM. The relative bandwidth of the original AM is 66% over 6.4–12.7 GHz, within which S_{11} is below than −10 dB. In addition, the minimum value is −30 dB at 8.6 GHz. It is obvious that the FSS presents band-stop characteristics in the vicinity of 12.7 GHz, 14.5 GHz and 15.7 GHz. The electromagnetic waves at these frequency points are almost reflected. The selection reflection increased the absorbing characteristic at higher frequency. When FSS is embedded below the AM structure with a substrate-supported FSS, $S_{11} < -10$ bandwidth is broadened to 112% covering 3.9–13.9 GHz, with three valleys of −14 dB at 4.2 GHz, −25 dB at 6.4 GHz and −16.5 dB at 9.5 GHz, respectively. Figure 2(b) illustrates the absorption comparison of the original AM with the proposed WAM. In the vicinity of 6.4 GHz, the absorption rate of composite WAM is approximate to 100% and the optimal absorption rate is over 90% over C and X bands. Compared with absorber of the same mechanism, the bandwidth in this paper is wider, and the total thickness is relatively small, which is better than the recent work in [17, 18] (see Table 2).

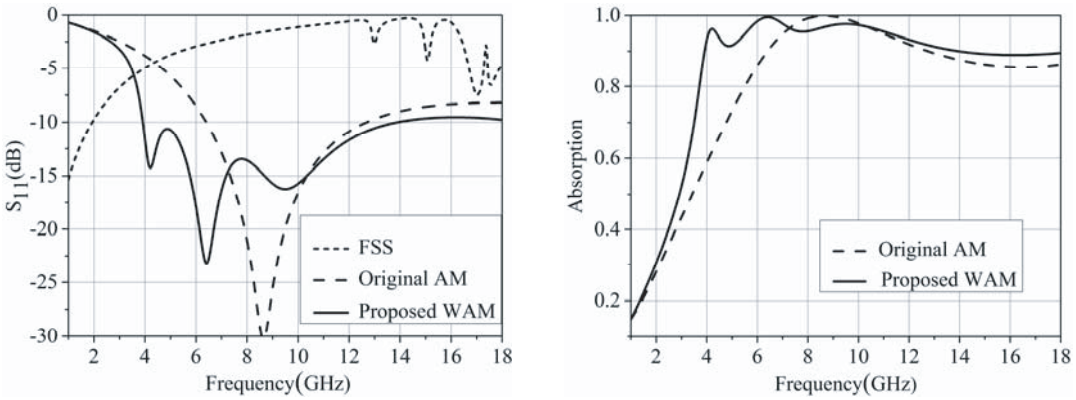

Figure 2. (a) Reflection of the original AM, FSS and proposed WAM. (b) Absorption comparison of the original AM with the proposed WAM.

Table 2. Comparison of the absorbing characteristics.

Reference	Absorbing band	Total thickness	f_{max}/f_{min}	Relative bandwidth
Ref. [12]	4.5–12.53 GHz	2.70 mm	2.78	94.3%
Ref. [17]	7.8–24 GHz	3.13 mm	3.07	108%
Ref. [18]	8–18 GHz	1.80 mm	2.25	77%
This paper	3.9–13.9 GHz	2.50 mm	3.56	112%

Figure 3 gives the magnetic fields comparisons of the original AM with proposed WAM, and vector plot of the surface current density in FSS. It can be seen that strong currents flow through across FSS at 4.2 and 6.4 GHz. The magnetic field intensities in the original magnetic sheet are small, and have

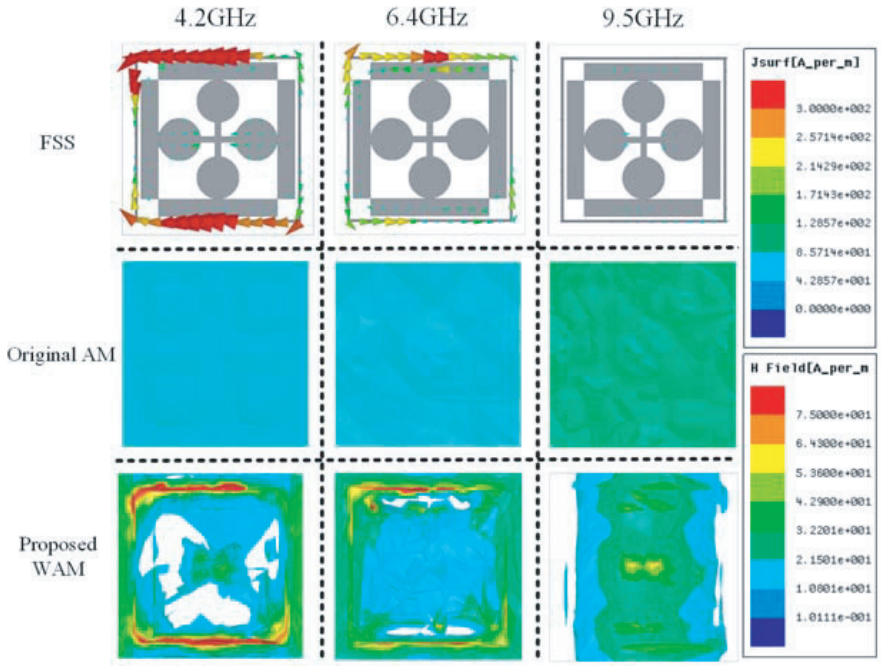

Figure 3. Vector plot of the surface current density in FSS and magnetic fields in two AMs at 4.2, 6.4, and 9.5 GHz.

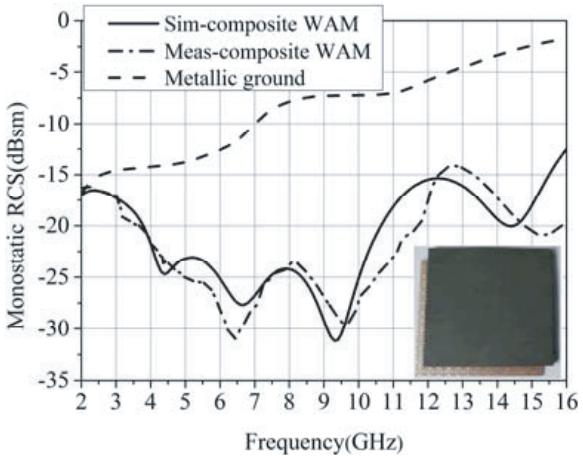

Figure 4. Simulated and measured RCS of composite WAM with metallic plate.

been greatly enhanced where the maximum currents flow through. Thus efficient absorbing performance is obtained by magnetic resonances in the low frequency band after FSS is embedded. In addition, a degradation of the magnetic field at 9.5 GHz is found, but there is still a good wave absorbing property.

Based on the above approach, a 13×13 unit cells composite WAM reflective screen and a metallic plate of the same size are fabricated. The simulated and measured monostatic RCS curves are shown in Figure 4, when a normal incident plane wave irradiates on the metallic plate and the composite WAM. It can be seen that the monostatic RCS reduction at 9.4 GHz is up to 24 dB and the average reduction in the desired frequency range is above 10 dB. The measured RCS is in good agreement with the simulated one. Furthermore, comparison of simulated RCS as a function of the incident angle at 6.4 GHz and 9.4 GHz are given in Figure 5. As is apparent, the monostatic RCS reduction is realized in the angular region $-80^\circ \leq \theta \leq 80^\circ$ except for individual angles.

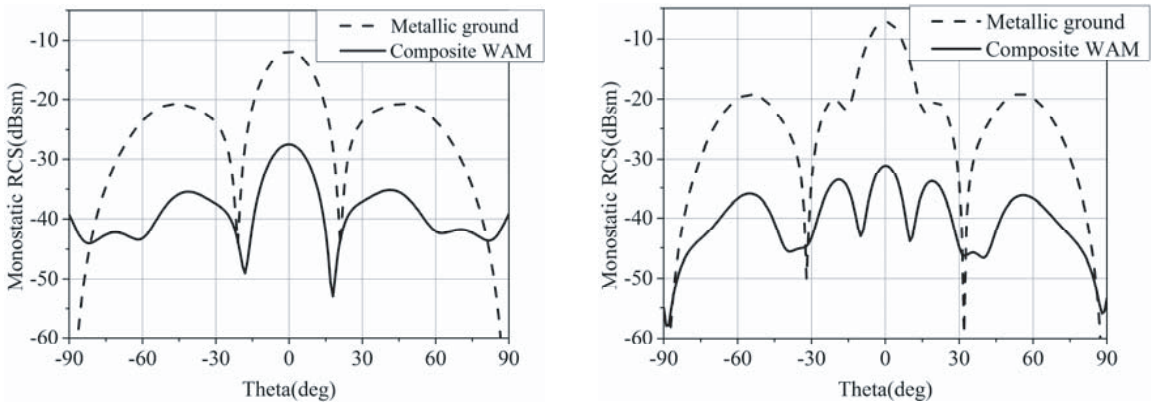

(a) (b)

Figure 5. Comparisons of simulated RCS versus the incident angle at (a) 6.4 GHz and (b) 9.4 GHz.

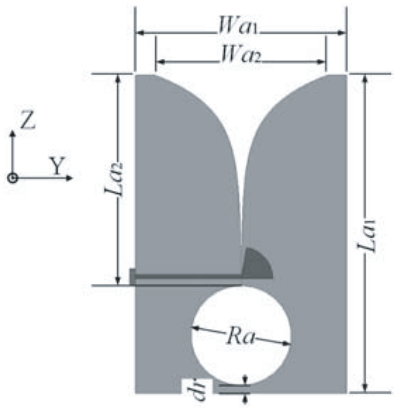

Figure 6. The geometry of the Vivaldi antenna.

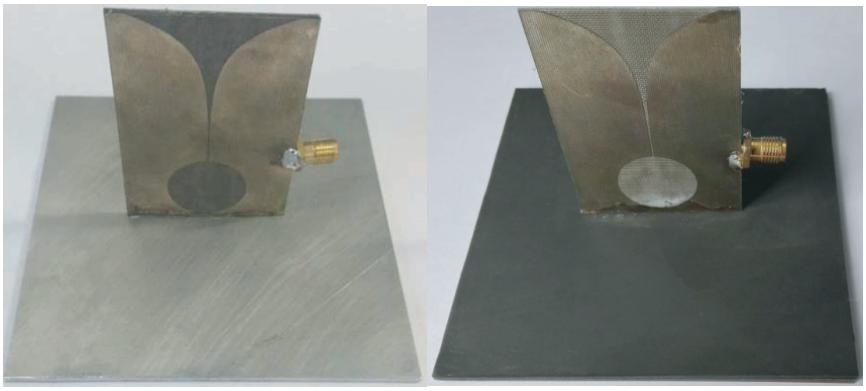

(a) (b)

Figure 7. Photographs of (a) reference antenna and (b) proposed antenna.

3. WAM-BASED LOW-RCS ANTENNA

The configuration of the original Vivaldi antenna is illustrated in Figure 6, and $La_1 = 60.5\,\text{mm}$, $Wa_1 = 40\,\text{mm}$, $La_2 = 40\,\text{mm}$, $Wa_2 = 30\,\text{mm}$, $Ra = 19\,\text{mm}$, $dr = 1.5\,\text{mm}$. An original Vivaldi antenna consists of three parts, namely the feed structure, tapered slot line and metallic layer which are fabricated on the two sides of the substrate ($\varepsilon_r = 2.65$, $\tan\delta = 0.0025$) with a thickness of 1 mm. In addition, the feed line is in the middle of the substrates, and the antenna is fed by a coaxial line. Aiming to improve the bandwidth of the antenna, a fan-shaped microstrip stub is utilized in the feed line. By properly optimizing the dimensions of the composite WAM, its operating band can cover the impedance bandwidth of the Vivaldi antenna. For comparisons, the ground plane of the reference antenna is as large as the composite WAM of the proposed antenna. As an application example, a Vivaldi antenna with metallic ground plane is selected to be the reference antenna. To validate WAM's contribution in RCS reduction, the difference of proposed antenna is that the metallic ground has been replaced by the composite WAM. The first layer of the WAM is the black gummed rubber AM, under which the FSS is printed. Photographs of both antennas are given in Figure 7.

3.1. Simulated and Measured Radiation Characteristics

The impedance characteristics of two antennas were tested with the Agilent E5071C vector network analyser. Furthermore, we completed the measurement of radiation patterns in the SATIMO SG24-L

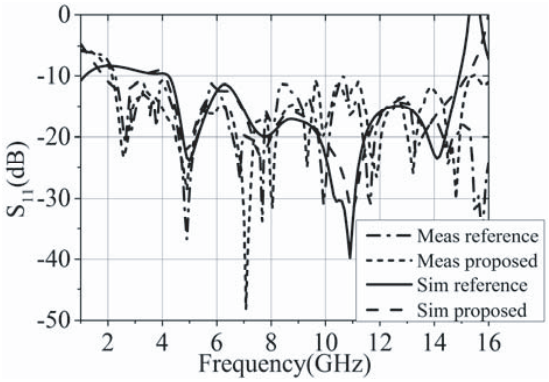

Figure 8. Comparison of simulated and measured reflection curves.

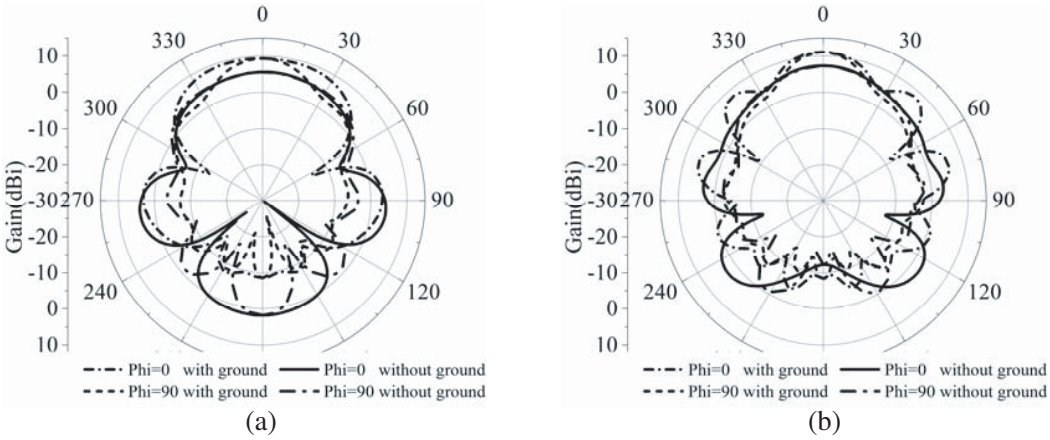

Figure 9. Comparison of the simulated radiation patterns between antenna with and without the metal sheet at (a) 7 GHz (b) at 9 GHz.

anechoic chamber. Figure 8 shows the simulated and measured frequency response of two antennas. Due to the fabrication tolerance and measurement uncertainty, it can be seen that some frequency points of the proposed antenna are slightly higher than the reference one, and there are more peaks in measured curves. The simulated operating band is 4.6–14.9 GHz while the measured one is 2.3–15 GHz. The measured antenna bandwidth is a little wider than the simulation one. Even so, it is obvious that S_{11} of the antenna with two different ground planes is basically consistent.

Radiation comparisons between the antenna with and without the metal sheet at 7 GHz and 9 GHz are given in Figure 9. It is obvious that the backward gain of antenna with metallic ground is obviously reduced, and the forward gain is increased. The measured radiation patterns in two orthogonal planes of the Vivaldi antenna with different ground planes at 10.3 GHz are shown in Figure 10, respectively. It can be seen that the gain in normal direction (z-axis) decreases from 9.16 dBi to 8.52 dBi, and the gain loss is 0.64 dB. Compared with the reference antenna, the gain of the antenna is decreased in the range of available frequencies. However, the gain loss that is less than 1 dB in low-RCS antenna design is considered acceptable. So we can draw a conclusion that the radiation patterns of the proposed antenna do not degrade obviously. Besides, the measured radiation patterns are in good agreement with simulation ones. In a word, the radiation characteristics of the Vivaldi antenna are basically preserved when the composite WAM plane is used.

3.2. Simulated and Measured Scattering Characteristics

In an anechoic chamber for scattering field measurement, shown in Figure 11, six pairs of horn antennas are selected as emitters and receivers to cover the frequency band from 2 to 18 GHz. The emitter

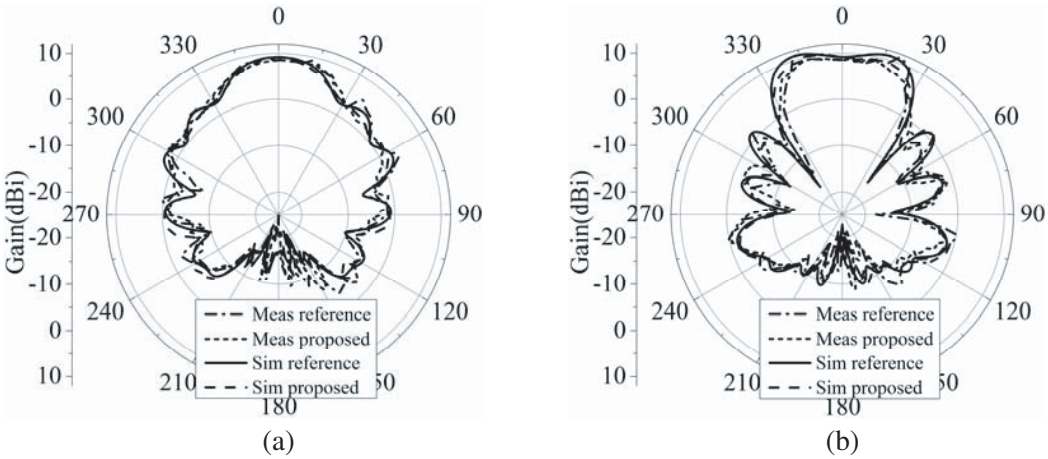

Figure 10. Comparison of radiation patterns at 10.3 GHz in (a) XoZ-plane, and (b) YoZ-plane.

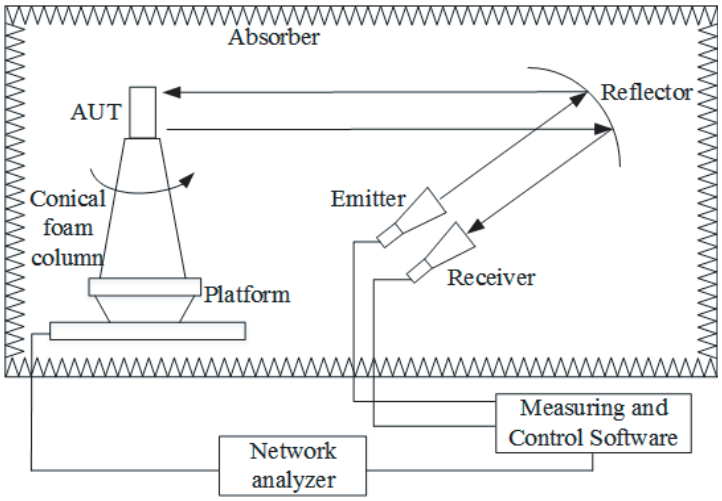

Figure 11. Skematic view of the compact scattering measurement setup in an anechoic chamber.

radiates the electromagnetic wave (EM), and then the EM wave is reflected by the reflector to form a quasi-plane wave. The object under test is terminated with matched loads and illuminated by the incoming wave. And then the scattering wave versus frequency and for each rotating angles can be received by the receiver.

Figure 12 shows the comparison of the monostatic RCSs of the Vivaldi antenna with two different ground planes, with the incident wave perpendicular to the ground plane. It is obvious that the RCS of Vivaldi antenna with the composite WAM is reduced over the whole operation band. Besides the C and X bands, working bands of the composite WAM, reduction in different degrees can be found in adjacent bands. The simulation results show that the average RCS reduction is greater than 5 dB ranging from 2–18 GHz, and the maximum reduction is 16 dB at 11.5 GHz.

Furthermore, comparisons of monostatic RCSs as a function of incident angles from $-90°$–$90°$ at two orthogonal planes at 8.3 GHz are given in Figure 13. It can be seen that over $-80° \leq \theta \leq 80°$, there is an excellent RCS reduction in the whole angular region except minority angles. Good agreement is obtained between the simulated and measured results. Some discrepancies may come from the fabrication tolerance and misalignments in the measurement setup. In addition, the shift in zero-direction is in virtue of the fact that deviation of position is inevitable when RCS versus the incident angles is measured.

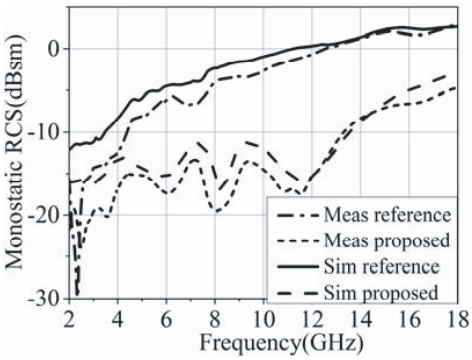

Figure 12. Comparison of monostatic RCSs between the reference and proposed antenna for a normal incident plane wave in x-polarization.

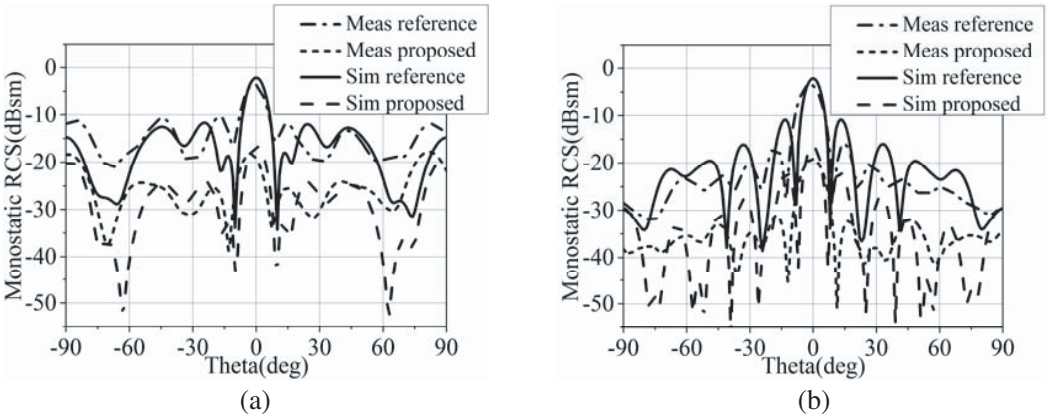

Figure 13. Simulated and measured monostatic RCS under various angles of impinging waves in x-polarization at 8.3 GHz in (a) XoZ-plane and (b) YoZ-plane.

4. CONCLUSION

In this paper, a dual-band composite WAM based on FSS is presented, and the absorbing bandwidth has been broadened significantly from 66% to 112%, showing good absorbing characteristics over the C and X bands. Moreover, the metallic ground plane of a Vivaldi antenna is replaced by the composite WAM to verify its contribution in RCS reduction. Experimental and simulated results prove that considerable RCS reduction can be realized in a broadband and over wide incident angles, with the largest reduction 16 dB at 11.5 GHz. The results exhibit that this method is effective to obtain in-band antenna RCS reduction over broadband and wide angular range.

REFERENCES

1. Seman, F. C., R. Cahill, and V. Fusco, "Salisbury screen absorber with angular and polarization insensitive resonant frequency" *European Conference on Antenna and Propagation (EUCAP)*, 1556–1559, 2009.
2. Zhang, J. J., J. H. Wang, M. Chen, and Z. Zhang, "RCS reduction of patch array antenna by electromagnetic band-gap structure," *IEEE Antennas Wireless Propag. Lett.*, Vol. 11, 1048–1051, 2012.
3. Wang, F.-W., S.-X. Gong, S. Zhang, X. Mu, and T. Hong, "RCS reduction of array antennas with radar absorbing structures," *Journal of Electromagnetic Waves and Applications*, Vol. 25, No. 17–18, 2487–2496, 2012.

4. Zhu, B., Z. Wang, C. Huang, Y. Feng, J. Zhao, and T. Jiang, "Polarization insensitive metamaterial absorber with wide incident angle," *Progress In Electromagnetics Research*, Vol. 101, 231–239, 2010.
5. Cheng, Y.-Z., Y. Wang, Y. Nie, R.-Z. Gong, X. Xiong, and X. Wang, "Design, fabrication and measurement of a broadband polarization-insensitive metamaterial absorber based on lumped elements," *J. Appl. Phys.*, Vol. 111, No. 4, 509, 2012.
6. Fallahzadeh, S., K. Forooraghi, and Z. Atlasbaf, "Design, simulation and measurement of a dual linear polarization insensitive planar resonant metamaterial absorber," *Progress In Electromagnetics Research Letters*, Vol. 35, 135–144, 2012.
7. Kollatou, T. M., A. I. Dimitriadis, S. D. Assimonis, N. V. Kantartzis, and C. S. Antonopoulos, "A family of ultra-thin polarization insensitive multi-band highly absorbing metamaterial structures," *Progress In Electromagnetics Research*, Vol. 136, 579–594, 2013.
8. Zhang, C.-F., W. Tang, X.-L. Mi, and L.-R. Chen, "Application of radar absorbing material in design of metal space frame radomes," *Cross Strait Quad-Regional Radio Science and Wireless Technology Conference (CSQRWC)*, Vol. 1, 222–225, 2011.
9. Wang, W.-T., S.-X. Gong, X. Wang, H.-W. Yuan, and J. Ling, "RCS reduction of array antenna by using bandstop FSS reflector," *Journal of Electromagnetic Waves and Applications*, Vol. 23, No. 11–12, 1505–1514, 2009.
10. Chen, Q., J. J. Jiang, X. X. Xu, Y. He, and L. Chen, "Thin and broadband electromagnetic absorber design using resistors and capacitors loaded frequency selective surface," *Journal of Electromagnetic Waves and Applications*, Vol. 26, No. 16, 2102–2111, 2012.
11. WasifNiaz, M., R. A. Bhatti, and I. Majid, "Design of broadband electromagnetic absorber using resistive Minkowski loops," *International Burbank Conference on Applied Sciences & Technology (IBCAST)*, 424–428, 2013.
12. Lv, J., S.-X. Gong, F.-W. Wang, J. Luo, and Y.-X. Zhang, "RCS reduction of Quasi-Yagi antenna," *Progress In Electromagnetics Research C*, Vol. 53, 89–97, 2014.
13. Wang, F.-W., W. Jiang, T. Hong, H. Xue, S.-X. Gong, and Y.-Q. Zhang, "Radar cross section reduction of wideband antenna with a novel wideband radar absorbing materials," *IET Microw. Antennas Propag.*, Vol. 8, No. 7, 491–497, 2014.
14. Teni, G., N. Zhang, J. Qiu, and P. Zhang, "Research on a novel miniaturized antipodal Vivaldi antenna with improved radiation," *IEEE Antennas Wireless Propag. Lett.*, Vol. 12, 417–420, 2013.
15. Yan, J.-B., G. Sivaprasad, C.-R. Bruno, and B. John, "A dual-polarized 2–18-GHz vivaldi array for airborne radar measurements of snow," *IEEE Trans. Antennas Propag.*, Vol. 64, No. 2, 781–785, 2016.
16. Saptarshi, G., "An equivalent circuit model of FSS-based metamaterial absorber using coupled line theory," *IEEE Antennas Wireless Propag. Lett.*, Vol. 14, 511–514, 2015.
17. Zabri, S. N., R. Cahill, and A. Schuchinsky, "Compact FSS absorber design using resistively loaded quadruple hexagonal loops for bandwidth enhancement," *Electronics Letters*, Vol. 51, No. 2, 162–164, 2015.
18. Yang, Z.-N., F. Luo, L. Gao, Y.-C. Qing, W.-C. Zhou, and D.-M. Zhu, "Enhanced microwave absorption properties of carbon black/silicone rubber coating by frequency-selective surface," *Journal of Electronics Materials*, Vol. 45, No. 10, 5017–5023, 2016.